Structure and Dynamics of Penumbral Filaments

B. Ruiz Cobo, and L.R. Bellot Rubio

Abstract High-resolution observations of sunspots have revealed the existence of dark cores inside the bright filaments of the penumbra. Here we present the stationary solution of the heat transfer equation in a stratified penumbra consisting of nearly horizontal magnetic flux tubes embedded in a stronger and more vertical field. The tubes and the external medium are in horizontal mechanical equilibrium. This model produces bright filaments with dark cores as a consequence of the higher density of the plasma inside the flux tube, which shifts the surface of optical depth unity toward higher (cooler) layers. Our results suggest that the surplus brightness of the penumbra is a natural consequence of the Evershed flow, and that magnetic flux tubes aobut 250 km in diameter can explain the morphology of sunspot penumbra.

1 Introduction

A good knowledge of the structure of the penumbra is important to understand various physical processes occurring in sunspots as, for example, the Evershed flow, the brightness of the penumbra, and the coexistence of magnetic fields with different strengths and inclinations. Despite significant advances in the characterization of the penumbra during the last years [15, 1, 2], its basic building blocks have not been identified unambiguously as yet.

Recent images taken with the Swedish 1-m Solar Telescope have demonstrated that many penumbral filaments possess internal structure in the form of a dark core [12, 10, 20]. The central obscuration is surrounded by two narrow lateral brightenings, both of which are observed to move with the same speed and direction as a single entity.

The origin of these structures remains enigmatic. In a recent paper, Spruit & Scharmer [18] examined the idea that dark-cored filaments could be the signature of field-free gaps just below the visible surface of the penumbra. They suggested that the top of the gaps would be observed as dark cores due to their increased plasma

B. Ruiz Cobo,
Instituto de Astrofísica de Canarias, Tenerife, Spain e-mail: brc@iac.es

L.R. Bellot Rubio,
Instituto de Astrofísica de Andalucía (CSIC), Granada, Spain e-mail: lbellot@iaa.es

density that shifts the $\tau = 1$ level to higher (cooler) layers. They also speculated that the large variations of the magnetic field strength and inclination around and above the gaps could explain the net circular polarization of spectral lines observed in the penumbra. For the moment, no radiative transfer calculations have been performed to sustantiate these claims.

On the other hand, the idea that a dark-cored penumbral filament represents a magnetic flux tube embedded in a stronger and more vertical ambient field is very appealing. This model of the penumbra, known as the uncombed model [16], has been used with great success to reproduce the polarization profiles of visible and infrared spectral lines emerging from sunspots. Numerical simulations of the evolution of penumbral flux tubes have been carried out by, e.g., Schlichenmaier [13]. The simulations offer an explanation for the existence of the Evershed flow and explain, at least qualitatively, the most important features of the penumbra. Given the success of the uncombed model, it seems natural to examine whether it can also explain the existence of dark-cored filaments.

Schlichenmaier et al. [14] studied the radiative cooling of hot penumbral flux tubes surrounded by a non-stratified, initially isothermal atmosphere. They found that the tubes cool down very quickly in the absence of energy sources, reaching thermal equilibrium with the external medium in only a few tens of seconds. No dark cores would be observed under these conditions.

Here we extend the work of Schlichenmaier et al. [14] by solving the stationary heat transfer equation in a 2D stratified penumbra. We model penumbral filaments as magnetic flux tubes embedded in a stronger and more vertical ambient field. The two sources of energy we consider are Ohmic dissipation and a hot Evershed flow. Our calculations show that the temperature distribution is not symmetric around the tube axis, and that one such tube would be observed as a dark-cored filament due to the higher density (hence higher opacity) of the plasma within the tube. Interestingly, the observed intensity contrast of the dark core relative to the surroundings is not well reproduced without the Evershed flow. More details about the equations, numerical methods, results, and implications can be found in [11].

2 The model

We describe a bright penumbral filament as a cylindrical magnetic flux tube of radius R embedded in a stratified background atmosphere. Spectropolarimetric observations suggest that the inclination and strength of the magnetic field are different in the tube and the external medium. This produces electrical currents at the interface. We account for them assuming that the tube and the surrounding atmosphere are separated by a current sheet of thickness δ which extends from $r = R - \delta$ to $r = R$.

We require the tube and the surroundings to be in lateral mechanical equilibrium, i.e., the total (gas plus magnetic) pressures inside and outside the tube must be the same at the same geometrical height z. The ideal gas law then determines the gas density if the temperature and the magnetic field strength are known. The

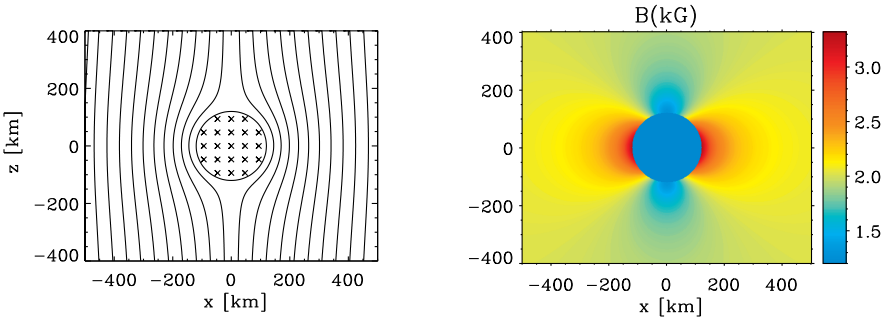

Fig. 1 *Left:* Magnetic field lines in the plane perpendicular to the tube's axis (the *xz* plane). The circle centered at $z = 0$ represents the tube's boundary. *Right:* Field stregth distribution.

temperature distribution is obtained by solving the stationary heat transfer equation. Since the only purpose of the present calculations is to identify the physical mechanism responsible for the existence of dark cores, we adopt the simplest magnetic configuration possible, namely a potential field. The field is determined from the conditions $\nabla \cdot \mathbf{B} = 0$ and $\nabla \times \mathbf{B} = 0$ in the *xz*-plane, i.e. we neglect variations along the tube axis because they are much smaller than variations perpendicular to it [4]. In the tube's interior, the field is assumed to be homogeneous and directed along its axis. Figure 1 shows the magnetic configuration of the model with $R = 120$ km, $B_\mathrm{t} = 1200$ G, $\gamma_\mathrm{t} = 90^\circ$, $B_\mathrm{b} = 2000$ G, and $\gamma_\mathrm{b} = 40^\circ$. Note that the field lines in the background wrap around the tube, leading to enhanced field strengths on either side of the tube and a reduction of the field right above and below it. Note also that the field component normal to the tube's boundary vanishes, implying that the inclination of the external field does not remain constant. In particular, immediately above the tube the background field is more horizontal than γ_b.

3 Heat transfer equation

We solve the stationary heat transfer equation, $\nabla \cdot \mathbf{F} = S$, where $\mathbf{F} = \mathbf{F}_\mathrm{r} + \mathbf{F}_\mathrm{c}$ is the total energy flux (with $\mathbf{F}_\mathrm{r}$ the radiative flux and $\mathbf{F}_\mathrm{c}$ the convective flux), and S represents the various energy sources, including Joule heating and heat deposited by the Evershed flow. The radiative flux is computed using the diffusion approximation (e.g., [7]), i.e., $\mathbf{F}_\mathrm{r} = -k_\mathrm{r} \nabla T$, with k_r the radiative thermal conductivity and T the temperature. Following [14], we take $k_\mathrm{r} = 16 D_\mathrm{F} \sigma T^3 / (\kappa_\mathrm{R} \rho)$, where σ is Stefan-Boltzmann constant, κ_R the Rosseland mean opacity, ρ the plasma density, and D_F the flux limiter originally introduced by Levermore & Pomraning [6]. For the calculation of the convective flux we adopt a linearized mixing length approach [8] and use $\mathbf{F}_\mathrm{c} = -k_\mathrm{c} \left[\nabla T - (\mathrm{d}T/\mathrm{d}z)_\mathrm{ad} \right]$. The quantity $(\mathrm{d}T/\mathrm{d}z)_\mathrm{ad} = T(\mathrm{d}P/\mathrm{d}z)\nabla_\mathrm{ad}$ rep-

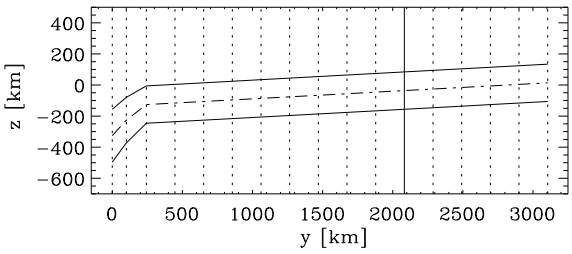

Fig. 2 Cut of the computational domain at x=0 km, showing a tube 120 km in radius. The vertical lines mark the 17 *xz*-planes where we solve the heat transfer equation. The line at *y*=2083 km indicates the position of the *xz*-cut displayed in Fig. 3

resents the adiabatic temperature gradient and $\nabla_{\rm ad}$ the double-logarithm isentropic temperature gradient. The convective transport coefficient $\kappa_{\rm c}$ is calculated using the linearized approximation of Spruit [17].

The heat transfer equation is solved numerically with Neumann boundary conditions given by $\delta T(x,z=0)=0\,\forall x$ and $\delta\dot{T}(x=0,z)=\delta\dot{T}(x=L,z)=0\,\forall z$. Here, δT stands for temperature departures from the solution without tube. The second condition forces the temperature perturbations to be minimum at the lateral boundaries of the computational domain.

3.1 Simulation setup

The computational box is a cube extending 1000 km in the *x*-direction, 3100 km in the *y*-direction, and 1200 km in the *z*-direction. Initially, the cube is filled with an unperturbed atmosphere (the cool model of Collados et al. [5]) with magnetic field strength $B_{\rm b}=2000$ G and field inclination $\gamma_{\rm b}=40^\circ$. A penumbral flux tube is embedded in this atmosphere. The tube has a radius $R=120$ km, a current sheet 2 km thick, a field strength $B_{\rm t}=1200$ G, and magnetic field inclinations varying between 45° and 87° as shown in Fig. 2. The axis of the tube is placed at a height determined by the field inclination and the distance along the tube, starting with $z=-326$ km at $y=0$ km.

The 2D stationary heat transfer equation has been solved in 17 *xz*-planes at different *y* values (cf. Fig 2). Each plane is discretized in 501×601 grid points, the step size being 2 km.

4 Results and discussion

The Evershed flow is a radial, nearly horizontal mass outflow observed in sunspot's penumbrae. It is associated with the more inclined magnetic field component of the penumbra [21, 19, 22, 1, 9] and often exhibits supersonic velocities [3]. The Evershed flow has been modeled as a material flow along thin flux tubes [13].

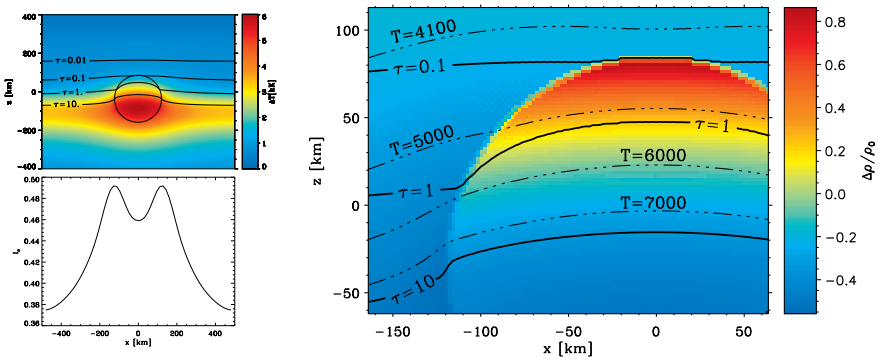

Fig. 3 Top left panel: Temperature perturbation δT in the xz–plane at $y = 2083$ km. The sources of energy are Ohmic dissipation and a hot Evershed flow. The circle represents the flux tube. Solid lines are lines of constant Rosseland optical depth. Bottom left panel: continuum intensity at 487.8 nm emerging from the $y = 2083$ km plane, convolved with the Airy point-spread function of a 1-m telescope. The values are normalized to the quiet Sun continuum intensity. Right panel: Section of the same plane showing gas density perturbations $\Delta\rho/\rho_0$ induced by the weaker field of the tube and the Evershed flow. Dash-dotted lines represent isotherms. Solid lines indicate lines of constant Rosseland optical depth.

An Evershed flow of hot plasma along a magnetic flux tube with velocity $\mathbf{v}_\mathrm{E}$ produces a flux of energy $\mathbf{F}_\mathrm{E}$ whose divergence can be evaluated from the entropy equation as

$$\nabla \cdot \mathbf{F}_\mathrm{E} = \rho c_V \mathbf{v}_\mathrm{E} \left[\nabla T - (\mathrm{d}T/\mathrm{d}z)_\mathrm{ad} \mathbf{e}_\mathrm{z}\right], \tag{1}$$

where c_V is the specific heat at constant volume. To account for the heating induced by the Evershed flow, we set $S = j^2/\sigma + \nabla \cdot \mathbf{F}_\mathrm{E}$ in the stationary heat transfer equation. We assume that the Evershed flow is parallel to the magnetic field inside the tube ([3]), and that its velocity changes with radial distance as dictated by mass conservation due to the decrease of the density with height.

Figure 3 shows the results of the calculations for the xz-plane at $y = 2083$ km, assuming v_E to be 7 km s^{-1} at $y = 0$ km. As can be seen in the upper left panel, the Evershed flow causes an intense heating of the tube and the surroundings. The right panel demonstrates that the $\tau_\mathrm{R} = 1$ level is shifted upwards within the flux tube. The reason is the weaker field of the tube, which increases its density and opacity. The $\tau_\mathrm{R} = 1$ level then moves to higher layers, where the temperature is lower. This produces a dark-cored penumbral filament (cf. the lower left panel of Fig. 3).

Figure 4 displays a continuum image of the flux tube at 487.8 nm as it would be observed through a 1-m telescope at disk center ($\mu = 1$). This image has been obtained solving the radiative transfer equation for all xz-planes of the computational box. Note that the observed characteristics of dark-cored penumbral filaments are qualitatively well reproduced: the central obscuration is flanked by two lateral brightenings, the intensity of the dark core is about 85% that of the lat-

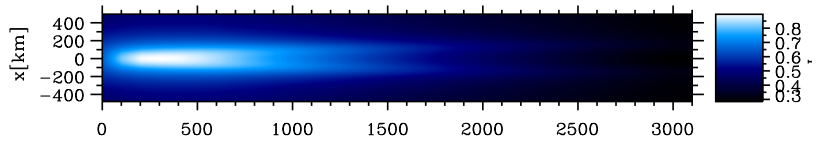

Fig. 4 Continuum image of the flux tube at 487.8 nm. The Evershed flow has a velocity of 7 km s^{-1} and induces a temperature excess of 7500 K within the tube at y=0 km.

eral brightenings, and the whole filament is significantly brighter than its surroundings [12, 20, 10].

The calculations presented here strongly support the view that the penumbra is formed by small (but thick) magnetic flux tubes, as inferred from the analysis of high resolution filtergrams and spectropolarimetric measurements [16, 15, 1].

Acknowledgements This work has been supported by the Spanish Ministerio de Ciencia y Tecnología under projects AYA2001-1649, ESP2003-07735-C04-03, and *Programa Ramón y Cajal*

References

1. Bellot Rubio, L.R. 2004, Reviews in Modern Astronomy, 17, 21
2. Bellot Rubio, L.R. 2007, in Highlights of Spanish Astrophysics IV, ed. F. Figueras et al. (Dordretch: Springer), 271
3. Bellot Rubio, L.R., Balthasar, H., & Collados, M. 2004, A&A, 427, 319
4. Borrero, J.M., Solanki, S.K., Bellot Rubio, L.R., Lagg, A., Mathew, S.K. 2004, A&A, 422, 1093
5. Collados, M., Martínez Pillet, V., Ruiz Cobo, B., del Toro Iniesta, J.C., & Vázquez, M. 1994, A&A, 291, 622
6. Levermore, C.D., & Pomraning, G.C. 1981, ApJ, 248, 321
7. Mihalas, D. 1978, Stellar Atmospheres, Freeman and Co., San Francisco, p. 58
8. Moreno Insertis, F., Schüssler. M., & Glampedakis, K. 2002, A&A, 388, 1022
9. Rimmele, T. 2008, ApJ, 646, 593
10. Rouppe van der Voort, L.H.M., Löfdahl, M.G., Kiselman, D., Scharmer, G.B. 2004, A&A, 414, 717
11. Ruiz Cobo, B., & Bellot Rubio, L.R. 2008, A&A, 488, 749
12. Scharmer, G.B., Gudiksen, B.V., Kiselman, D., Löfdahl, M.G., & Rouppe van der Voort, L.H.M. 2002, Nature, 420, 151
13. Schlichenmaier, R., Jahn, K., Schmidt, H.U. 1998, A&A, 337, 897
14. Schlichenmaier, R., Bruls, J.H.M.J., Schüssler, M. 1999, A&A, 349, 961
15. Solanki, S.K. 2003, A&AR, 11, 153
16. Solanki, S.K., Montavon C.A.P., 1993, A&A, 275, 283
17. Spruit, H.C. 1977, Sol. Phys., 55, 3
18. Spruit, H.C., Scharmer, G.B. 2006, A&A, 447, 343
19. Stanchfield, D.C.H., Thomas, J.H. & Lites, B.W. 1997, ApJ, 477, 485
20. Sütterlin, P., Bellot Rubio, L.R., Schlichenmaier, R. 2004, A&A, 424, 1049
21. Title, A.M. Frank, Z.A., Shine, R.A., et al. 1992, ApJ, 403, 780
22. Westendorp Plaza, C., del Toro Iniesta, J.C., Ruiz Cobo, B., & Martínez Pillet, V., 2001, ApJ, 547, 1148